UNIVERSITY of York

This is a repository copy of *Elucidating the Role of Topological Constraint on the Structure of Overstretched DNA using Fluorescence Polarization Microscopy*.

White Rose Research Online URL for this paper:
https://eprints.whiterose.ac.uk/176268/

Version: Accepted Version

Article:
Backer, Adam S, King, Graeme A, Biebricher, Andreas S et al. (6 more authors) (2021) Elucidating the Role of Topological Constraint on the Structure of Overstretched DNA using Fluorescence Polarization Microscopy. The Journal of Physical Chemistry. pp. 8351-8361.

https://doi.org/10.1021/acs.jpcb.1c02708

Reuse
This article is distributed under the terms of the Creative Commons Attribution-NonCommercial-NoDerivs (CC BY-NC-ND) licence. This licence only allows you to download this work and share it with others as long as you credit the authors, but you can't change the article in any way or use it commercially. More information and the full terms of the licence here: https://creativecommons.org/licenses/

Takedown
If you consider content in White Rose Research Online to be in breach of UK law, please notify us by emailing eprints@whiterose.ac.uk including the URL of the record and the reason for the withdrawal request.

White Rose university consortium
Universities of Leeds, Sheffield & York

eprints@whiterose.ac.uk
https://eprints.whiterose.ac.uk/

Elucidating the Role of Topological Constraint on the Structure of Overstretched DNA using Fluorescence Polarization Microscopy

Invited submission to the W. E. Moerner Festschrift Special Issue

Adam S. Backer[1,*], Graeme A. King[2], Andreas S. Biebricher[3], Jack W. Shepherd[4,5], Agnes Noy[4], Mark C. Leake[4,5], Iddo Heller[3], Gijs J. L. Wuite[3], and Erwin J. G. Peterman[3,*]

[1]Apple Inc., 1 Apple Park Way, Cupertino, CA 95014, USA

[2]Institute of Structural and Molecular Biology, University College London, Gower Street, London WC1E 6BT, UK

[3]Department of Physics and Astronomy, LaserLaB Amsterdam, Vrije Universiteit Amsterdam, De Boelelaan 1081, 1081 HV Amsterdam, The Netherlands

[4]Department of Physics, University of York, York, YO10 5DD, UK

[5]Department of Biology, University of York, York, YO10 5DD, UK

*Correspondence should be addressed to both Adam S. Backer (email: a.s.backer@gmail.com) and Erwin J. G. Peterman (email: e.j.g.peterman@vu.nl)

Abstract

The combination of DNA force spectroscopy and polarization microscopy of fluorescent DNA intercalator dyes can provide valuable insight into the structure of DNA under tension. These techniques have previously been used to characterize S-DNA – an elongated DNA conformation that forms when DNA overstretches at forces >65 pN. In this way, it was deduced that the base pairs of S-DNA are highly inclined, relative to those in relaxed (B-form) DNA. However, it is unclear whether and how topological constraints on the DNA may influence the orientations of intercalated dye molecules, and thus the base-pair inclinations. Here, we apply polarization microscopy to investigate the impact of DNA pulling geometry, torsional constraint and negative supercoiling on the orientations of intercalated dyes during overstretching. In contrast to earlier predictions, the pulling geometry (namely whether the DNA molecule is stretched via opposite strands or the same strand) is found to have little influence. However, torsional constraint leads to a substantial reduction in intercalator tilting in overstretched DNA, particularly in AT-rich sequences. Surprisingly, the extent of intercalator tilting is similarly reduced when the DNA molecule is negatively supercoiled, up to a critical supercoiling density (corresponding to ~70% reduction in linking number). We attribute these observations to the presence of P-DNA (an overwound DNA conformation). Our results suggest that intercalated DNA preferentially flanks regions of P-DNA rather than S-DNA and also substantiate previous suggestions that P-DNA forms preferentially in AT-rich sequences.

1. Introduction

Detailed knowledge of the elastic and mechanical properties of DNA is essential for obtaining a complete understanding of nucleic-acid processing *in vivo*. Under physiological conditions, and in the absence of force, double-stranded DNA exists in the so-called B-form, which exhibits a length of 0.34 nm/bp. However, when stretched to a force of ~65pN, B-DNA undergoes a structural transition known as overstretching [1, 2]. The overstretching transition (OST) is characterized by a 70% elongation of the DNA at nearly constant force, in which the double helix unwinds cooperatively, resulting in either base-pair-melted DNA, or an underwound, base-paired structure termed S-DNA. Whether S-DNA or melted DNA forms during overstretching depends on factors such as the base-pair sequence, ionic strength of the buffer and the temperature [3-8].

The case described above assumes that the DNA is torsionally unconstrained (UC), and thus that the molecule is topologically free to unwind under applied tension. The OST changes markedly when the DNA molecule is torsionally constrained (TC), due to fact that the overall linking number (*Lk*, defined as the sum of the twist and writhe in the molecule) must remain constant. Consequently, the OST in TC-DNA occurs at much higher forces (~110 pN) than for UC-DNA. This is because the presence of underwound structures (such as S-DNA) must be compensated for by a corresponding overwinding in other sections of the molecule [9]. It has been proposed that this local overwinding arises via the formation of a structure known as Pauling (P)-DNA, in which the phosphate backbones wrap around one another with a helicity of ~2.5 bases per turn. The bases in P-DNA are thought to be unpaired and point outwards [10]. Based on the measured helicity of S-DNA (~37.5 bp/turn), and the proposed structure of P-DNA, these two conformations are estimated to coexist in a ratio of approximately 4:1 S-DNA/P-DNA to ensure a constant *Lk* [9]. This finding was supported by subsequent fluorescence microscopy studies of

overstretched TC-DNA [11]. Owing to the increased stability of GC base-pairs relative to AT base-pairs, it was suggested that P-DNA (which requires base-pair melting) primarily forms in AT-rich sequences of the DNA molecule, while S-DNA dominates in GC-rich sequences [11].

When torsional stress is applied to TC-DNA, the overall *Lk* will either increase or decrease depending on the direction of the applied torque, resulting in DNA overwinding (positive supercoiling) or underwinding (negative supercoiling) respectively. The extent of supercoiling is defined by the relative change in *Lk*, parameterized by the supercoiling density, $\sigma = (Lk - Lk_0)/Lk_0$. Here, Lk_0 refers to the value of *Lk* in relaxed (B-form) DNA. In the case of negatively supercoiled DNA, less (overwound) P-DNA is required to offset (underwound) S-DNA during overstretching. At a critical supercoiling density of σ = -0.7, no P-DNA is required during overstretching and thus, at the end of the OST, the DNA will consist entirely of S-DNA [9].

In order to characterize local changes in the structure of overstretched DNA, fluorescence imaging and force spectroscopy of intercalated DNA has proved highly informative [4, 7, 12-14]. DNA intercalators are small planar dye molecules that bind to DNA by sliding between adjacent base pairs, which results in local unwinding and elongation of the double helix [15]. Upon binding to DNA, intercalators align parallel to neighboring base pairs and undergo a fluorescence enhancement of two orders of magnitude or more [16-18]. While intercalators strongly favor B-DNA binding, the absence of intercalator fluorescence has been used frequently to deduce the presence of non-B-form overstretched structures, such as S-DNA [4, 7, 11-14].

Polarized excitation and fluorescence imaging of intercalators can additionally reveal the orientations of the intercalated dyes' transition dipole moments relative to the axis of the DNA molecule. Previous studies have demonstrated that intercalated dyes orient perpendicular to the DNA-axis at forces < 65 pN and also for partially overstretched DNA (*i.e.* where less than 100%

of the molecule has been overstretched) [19-22]. In these cases, B-DNA neighboring the intercalation site acts to align the intercalators in the same orientation as the base pairs in B-form DNA. Recently [23, 24], we demonstrated that, at extensions beyond the end of the OST, intercalated dyes tilt to an orientation of $\theta \sim 54°$ relative to the DNA-axis. At these extensions, most of the B-DNA has been converted to S-DNA due to unwinding of the molecule. Although it is energetically unfavorable for intercalators to bind directly to S-DNA, our data suggested that dye molecules assume a tilted configuration when an intercalation site was neighbored by (unintercalated) S-DNA. Intercalator tilting was only observed at DNA extensions beyond the end of the OST, rather than during the OST (where S-DNA and B-DNA co-exist) because it is energetically unfavorable for S-DNA (relative to B-DNA) to neighbor intercalated DNA [14]. Taken together, these measurements led us to conclude that S-DNA exhibits highly inclined base pairs relative to B-DNA [24] and thus induces tilting of flanking intercalated DNA. While this work provided valuable insights into the structure of S-DNA, these experiments considered only a single stretching geometry in which the tension was applied via opposing 3' ends. However, it has been suggested that different base-paired overstretched structures may form depending upon whether tension is applied on the same or opposite DNA strands [25-30]. Moreover, the influence of torsional constraint and supercoiling (and thus the effect of P-DNA) on S-DNA-induced intercalator tilting is unknown.

Here, we apply intercalator polarization microscopy to explore the influence of pulling geometry, torsional constraint and negative supercoiling on the structure of overstretched DNA. We show that intercalator tilting beyond the OST in UC-DNA is independent of whether the construct is pulled via the 3' ends of opposite strands, or the 5' and 3' ends of the same strand. This indicates that the tilted orientation of intercalated dyes is caused by the inclined base pairs

within the S-DNA conformation and is not a consequence of a specific pulling geometry. We next demonstrate that at forces beyond the OST, intercalated dyes tilt significantly less in TC-DNA than in UC-DNA. Moreover, the extent of intercalator tilting in TC-DNA displays a strong sequence dependence, whereby dyes are tilted more strongly in GC-rich sequences compared with AT-rich DNA regions. This contrasts with the case of UC-DNA. Finally, we conducted similar fluorescence polarization measurements on negatively supercoiled TC-DNA using the recently reported technique of Optical DNA Supercoiling (ODS) [31]. These experiments reveal that over a narrow range of negative supercoiling densities ($-0.6 < \sigma < -0.7$), the intercalated dye orientations beyond the OST exhibit a sudden transition from a sequence-dependent, slightly-tilted state to a sequence-independent, highly-tilted state. From these results, we draw two main conclusions: First, we confirm that P-DNA forms predominantly within AT-rich sections of overstretched TC-DNA. Secondly, we argue that it is more favorable for P-DNA, rather than S-DNA, to flank intercalator binding sites.

2. Methods

2.i Polarization Microscopy

Fig. 1.A and 1.B provide an overview of the experimental technique. A setup combining dual-trap optical tweezers and fluorescence microscopy was used to manipulate and extend single DNA molecules, tethered between two optically trapped beads [32]. As described in Refs. [23, 24], polarized laser illumination was used for fluorescence excitation. However, in a departure from our previous work, fluorescence emission was *not* resolved into its X-/Y-polarized components (see our rationale behind this change in the paragraph below). As in our previous experiments [23, 24], we used bacteriophage λ DNA (λ-DNA), which has a contour length of ~16.5 μm. We used the bis-intercalator YOYO-1 to label the DNA. A collimated 488 nm laser beam was used for

widefield epifluorescence excitation. Laser intensities of ~1-5 W/cm^2 were used for imaging experiments (estimated by measuring transmitted laser power by placing a power-meter above the microscope objective and dividing by the size of the illuminated area at the sample). The polarization of the excitation laser was controlled using an EOM (model 350-80, Conoptics) placed in the beampath. By synchronizing the input voltage to the EOM with the camera exposure TTL signal, the excitation laser was rapidly toggled between X- and Y-polarization during the read-out period after each successive camera frame was recorded. Additionally, the intensity of the polarized excitation laser was controlled using a liquid crystal beam attenuator (ThorLabs LCC 1620) placed before the EOM. This device was modulated after each camera exposure to compensate for polarization-dependent losses incurred as the beam propagated through the excitation pathway, and achieve different intensities for X-/Y-polarized excitation (Fig. 1.A and B). The degree of polarization of the collimated excitation beam was measured to be >98%, and within ~2° of the X- and Y-axes of the experimental reference frame, using a polarimeter (ThorLabs PAX 1000VIS) placed above the microscope objective. Raw fluorescence data (Fig. 1.C) was acquired using an Andor EMCCD (iXON 897) set to an electron multiplication gain of 100, using integration times of 1 sec. per camera frame for both X-/Y-polarized excitation. A complete description of other aspects of the experimental apparatus may be found in previous work [24].

Here, we detail some key changes to our experimental approach that facilitated the study of TC-DNA and supercoiled DNA. A single nick in the DNA backbone will cause the entire construct to become torsionally unconstrained, irreversibly altering the force-extension behavior (Fig. 1.D) and limiting our ability to investigate conformations that require a fixed linking number before and during overstretching. Fluorescence imaging therefore had to be carried out under

conditions that minimize the risk of photo-induced nicking upon bleaching of intercalated dyes. Thus, it was paramount to limit the fluorescence excitation laser intensity and reduce fluorescence excitation of intercalated DNA. Due to the need to conserve dim fluorescence signal as much as possible, we departed from our previous approach by opting to not use a polarizing beamsplitter in the imaging pathway of our microscope. In this imaging configuration, we no longer resolve the polarization of light emitted by intercalated dye molecules, and instead rely on changes in total fluorescence intensity as a function of excitation polarization to gather information about the overall alignments of intercalated dyes [33-35]. This technique uses changes in fluorescence emission to determine how efficiently intercalated dyes absorb X- versus Y-polarized excitation light, and may be considered a *linear dichroism* measurement. The linear dichroism (LD) is calculated as:

$$LD = \frac{{}_{x}I - \varepsilon\, {}_{y}I}{{}_{x}I + \varepsilon\, {}_{y}I} \tag{1}$$

In Eqn. (1), ${}_{x,y}I$ are the background-subtracted fluorescence signals obtained using X-/Y-polarized excitation respectively (to maintain consistency with our earlier work, we use pre-scripts to denote excitation polarization, and omit post-scripts since the emission polarization is not resolved). ε is a correction factor that accounts for the difference in laser intensity used when alternately exciting with X-/Y-polarized illumination, as well as the polarization-dependent transmission efficiency of the filters placed in the imaging pathway. The LD alone does not enable the absolute orientation of the intercalated dyes to be determined (as this would require the combined excitation/emission polarization-resolved measurements, which are difficult to perform without nicking the DNA, as discussed above). Nevertheless, the LD provided a highly streamlined means of inferring relative changes in dye orientation. Specifically, the LD can be used to detect when dyes are no longer aligned in the plane perpendicular to the DNA-axis. Furthermore, the use

of a single (unpolarized) imaging channel enabled LD values to be calculated on a pixel-wise basis, without need for image registration – allowing spatial variations in LD along the axis of the DNA to be readily identified.

An additional modification to our experimental technique involved using substantially reduced laser power (ratio of 1:5.42) when exciting with Y-polarized as opposed to X-polarized illumination (Fig. 1.A and 1.B). The precise ratio of excitation power was determined by imaging a solution containing freely diffusing eGFP and measuring changes in fluorescence emission upon toggling the laser power/polarization. In conventional linear dichroism experiments, care is often taken to use near-equal excitation power for both excitation polarizations, leading to drastically different output intensities for well-ordered samples. In our case, however, increased output fluorescent signal went hand-in-hand with accelerated photo-nicking—it was therefore preferable to adjust the laser power such that fluorescent signal was uniformly low (yet still detectable above the background) for both input polarizations, and profit from a sufficiently low photo-nicking probability (allowing greater than ~ 8 seconds of imaging time in some cases). Since the TC-DNA constructs primarily exhibited negative LD (absorption dipole moments located primarily in the plane perpendicular to the DNA-axis), we reasoned that the laser power should be attenuated when using Y-polarized light to image an intercalated DNA molecule aligned along the Y-axis of the experimental system. This approach of using combined amplitude/polarization-modulation had the additional benefit of amplifying small changes in the fluorescence signal resulting from X-polarized excitation (which would cause unnecessary photo-nicking or even saturation of the camera sensor had identical power been used for the complementary Y-polarized excitation). The higher laser power used for X-polarized excitation was also necessary to obtain sufficient fluorescent signal above the background to make an accurate estimate of LD. For all fluorescence

imaging experiments, a ~25-50 nM concentration of the bis-intercalating dye YOYO-1 was used. YOYO-1 was selected because in our previous experiments [23, 24], intercalator tilting was most readily observed under a wide range of experimental conditions, due to the dye's slow unbinding kinetics at forces beyond the OST. A high-salt (1M NaCl) buffer was always used for imaging. This imaging buffer ensured that overstretching the DNA constructs would favor S-DNA formation as opposed to base-pair melting [7, 11].

2.ii DNA Construct Design and Generation of Negatively Supercoiled DNA

All experiments were performed using a linearized λ-DNA construct (~48.5 kb) which was end-labelled with biotin and tethered between streptavidin-coated microspheres (~4.5 μm, Spherotech). The topological state of these constructs varied depending on the biotin-labelling strategy. For opposite stranded constructs, biotin labels were added to the 3' ends of each strand, using Klenow DNA polymerase exo to fill in the 5' overhangs of λ-phage DNA with biotin-labelled nucleotides, as described previously [36]. For same-stranded UC constructs, biotins were positioned on the 3' and 5' ends of only one strand by ligating biotin-labelled oligonucleotides to each end of λ-phage DNA using the protocol detailed in Ref. [37]. Torsionally-constrained (TC) constructs were prepared by ligating a hairpin 'end-cap' to each end of linearized λ-DNA, such that both ends of the molecule were closed. Each end-cap was labelled with four biotins near the tip and, in most cases, the end-closed construct was tethered to streptavidin-coated beads via at least two biotins on each end of the molecule [11]. This prohibited rotation of the DNA molecule with respect to the beads and thus rendered the molecule torsionally constrained (note that the beads do not rotate in the optical traps).

The above end-capped TC-DNA construct was also used to generate negatively supercoiled molecules using Optical DNA Supercoiling (ODS) [31]. In brief, ODS exploits the mechanical

properties of end-capped TC-DNA to induce a fixed reduction in the overall *Lk*. This is achieved as follows: First, an end-capped TC-DNA molecule is stretched to forces >150 pN. After a period of time (typically 5-20 seconds) at these high forces, one or more biotin-streptavidin linkages are transiently broken, leaving one end of the DNA molecule tethered to the beads via only a single biotin-streptavidin tether. During this time, the molecule is in a torsionally unconstrained overstretched state. As a result, the *Lk* is reduced via swivelling of the DNA molecule around the single tether. When the broken biotin-streptavidin linkages re-form, the DNA molecule becomes torsionally constrained again, but with a lower *Lk* than that of B-form DNA. The reduced *Lk* is retained even when the tension is released, and therefore the molecule is negatively supercoiled. The extent to which *Lk* is reduced depends on the duration that the biotin-streptavidin bonds are broken for. Through repeated stretch-release cycles, the *Lk* can be reduced by between <5% and 70%. The supercoiling density can be quantitatively determined, based on the extension at which 70 pN of force is applied to the DNA molecule, using a look-up table that relates the DNA extension at 70 pN to the supercoiling density (see Fig. 2.B of Ref. [31]). In this way, the supercoiling density can be estimated with a precision of +/- 0.05 (however, factors such as the ionic strength of the imaging buffer and dye coverage can slightly bias these measurements). The maximum reduction in *Lk* is achieved when the entire DNA molecule is converted to S-DNA at high force through transient biotin-streptavidin ruptures of TC-DNA.

2.iii Data Analysis

LD measurements were performed on sequences of camera exposures at least two seconds long (one complete frame for both X-/Y-polarizations), and for some sequences as long as eight seconds (in which the four interleaved excitations using a given polarization were averaged together to yield an image with superior signal-to-noise). To perform *LD* measurement, the following

procedure was used: A region of interest (ROI) was specified using a custom Matlab GUI by selecting the end-points of a given DNA image (the locations where the DNA meets the trapped bead). The ROI was then defined as a line 5 camera pixels in diameter running between the two DNA end-points. Two regions of identical size containing only fluorescent background were automatically defined by offsetting the ROI by +/- 5 camera pixels, and smoothing out noise using a three-pixel Gaussian convolutional filter (sigma = 1 pixel). These two background regions were then averaged together to yield a pixel-wise map for background subtraction. Pixels containing background-subtracted signal less than a (heuristically chosen) threshold of 100 ADC counts were excluded from further analysis. This process was performed for both images corresponding to X-/Y-polarized signal using an identical ROI – permitting LD to be calculated on a pixelwise basis without need for image registration using Eqn. (1). Linear dichroism images were generated using a custom HSV colormap in which hue was used to denote LD, and the value was linearly scaled according to the fluorescence intensity ($_xI + \varepsilon\ _yI$). Regions of the image not containing the ROI were de-saturated (made black-and-white) to avoid distraction. To plot LD as a function of DNA position, the "Fractional DNA position" was defined as the position of a pixel relative to the end-points of an ROI, with 0 corresponding to the leftmost point and 1 corresponding to the rightmost. Individual pixels were plotted as dots with respect to their fractional position. To aid the viewer, smoothed data were also plotted as a solid line, using a Savitsky-Golay filter using default settings [38]. In this analysis, pixels having a fractional DNA position less than 0.05 or greater than 0.95 were excluded, since it was reasoned that the LD would be corrupted by the strong background signal emanating from the trapped beads. To compute the averaged LD across a portion of a DNA molecule, the mean LD from multiple pixels was determined, and confidence bars were drawn as the standard deviation, divided by the square-root of the number of pixels used to compute the

average. A given DNA molecule image generally contained ~1000 camera pixels used for *LD* calculation. To compute averaged *LD* in alternately GC-rich or AT-rich regions of the DNA [39], pixels with a fractional DNA position between 0.05 and 0.55 were designated as AT-rich, and those with a fraction position between 0.55 and 0.95 were designated as GC-rich. The orientation of the λ-DNA could be deduced by inspecting raw fluorescence images of TC-DNA obtained using X-polarized laser excitation and noting that one side of the λ-DNA (~45% of the entire construct) exhibited brighter emission (corresponding to the GC-rich region).

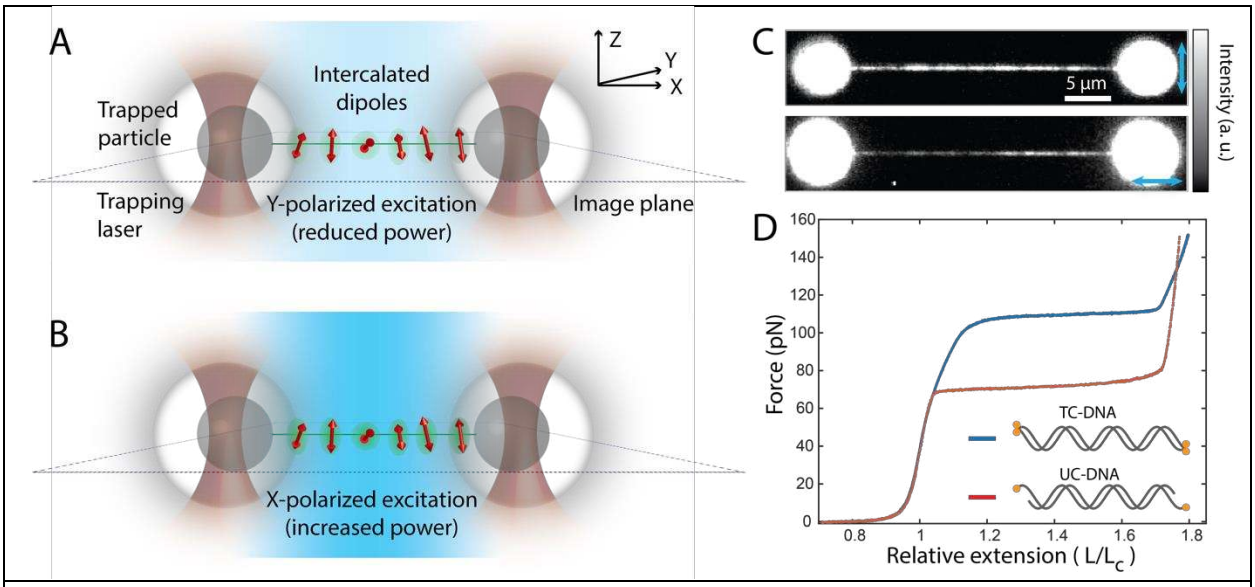

Fig. 1: Overview of the experimental method. (A) Imaging protocol: An intercalated λ-DNA molecule is stretched to a desired extension along the X-axis using dumbbell optical tweezers (transition dipole moments of intercalated dyes are drawn as red bidirectional arrows). The construct is first imaged using a reduced-power Y-polarized excitation beam, efficiently exciting dyes oriented close to the plane perpendicular to the DNA-axis (YZ-plane). (B) A second camera frame is recorded, using X-polarized light at increased power. This polarization will inefficiently excite dyes oriented in the YZ-plane but provide suitable fluorescence signal for *LD* measurement. (C) Representative fluorescence image data recorded using a TC-DNA molecule using Y-polarized (top) and X-polarized (bottom) excitation. (D) Representative force-extension curves for TC-DNA (blue) and UC-DNA (red). These curves were collected on DNA in the absence of intercalated dyes. Inset illustrates the attachment geometries for TC-DNA and UC-DNA constructs.

3. Results

3.i Same-Stranded Pulling Geometry Does Not Affect Intercalator Tilting

To assess the influence of attachment geometry (see Fig. 2.A) on the base-pair inclination in UC-DNA beyond the OST, we prepared λ-DNA constructs in which only one strand of the duplex DNA molecule was tethered to the beads by labelling the 3' and 5' ends of only one of the two complementary DNA strands with biotin (same-stranded pulling geometry). This contrasted with our earlier measurements, where the DNA molecule was labeled with biotin on the 3' ends of opposing strands (opposite-stranded pulling geometry) [23, 24]. We then stretched these constructs to beyond the OST in a high-salt buffer containing YOYO-1, and measured the LD as a function of applied force (Fig. 2.B). To ensure that the same-stranded pulling geometry was maintained throughout the LD measurements, it was important that photo-induced nicking of the tethered strand did not occur. Therefore, the DNA molecule was transferred to a low-salt (15 mM NaCl) buffer (in the absence of dye) after each fluorescence imaging experiment and then re-stretched. Under these conditions, strand peeling during overstretching is strongly favored over S-DNA formation, and thus for extensions beyond the OST ($L/L_c > 1.7$), the non-tethered strand will peel away from the tethered strand, yielding a purely single-stranded DNA construct (Fig. 2.C). However, if a nick was present in the tethered strand, the molecule would break during strand peeling. LD measurements were only considered for molecules where no nick was detected in the tethered strand. For nick-free molecules, LD measurements were collected under identical imaging conditions as for DNA attached using the opposite-stranded pulling geometry. To ensure that data sets were fully comparable, we recorded a new set of opposite-stranded stretching curves rather than using the data reported in [24]. Note that the nick-screening protocol described above for the same-stranded pulling geometry cannot be used for opposite-stranded pulling. However, in our

current and previous measurements [23,24], we have observed no indication that photo-nicking of a DNA molecule initially prepared for opposite-stranded pulling leads to a detectable change in fluorescence polarization or LD. Here, we observed very similar LD measurements for both pulling geometries, and in each case, we observe fluorescence depolarization at the end of the OST, as previously reported for the opposite-stranded pulling geometry [23, 24]. ANOVA analysis was performed by fitting a linear model to the plotted data, and the null hypothesis was confirmed (p-value of 0.27) [40]. Thus, the observed LD values at extensions beyond the OST indicate strong inclination of the DNA base pairs, independent of the specific attachment geometry.

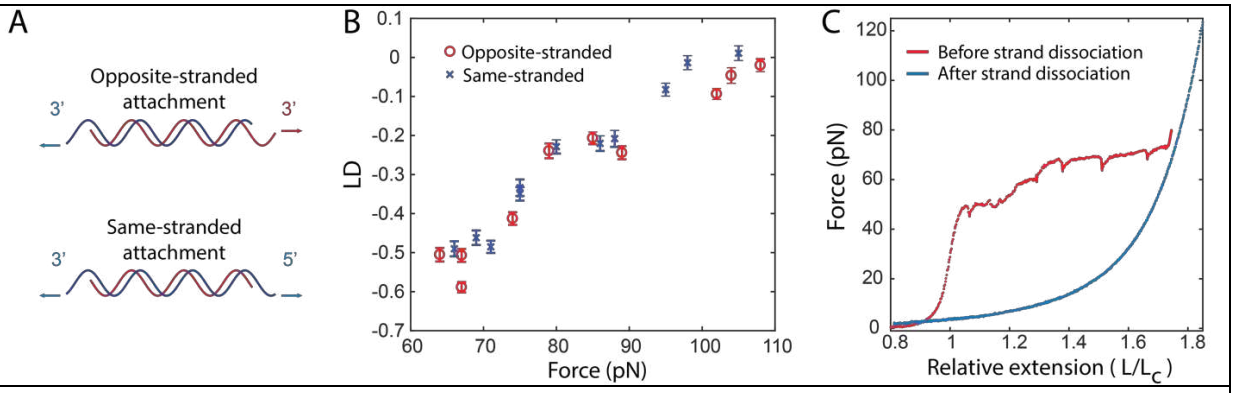

Fig. 2: Linear dichroism measurements of UC-DNA as a function of force for different pulling geometries. (A) Schematic of the DNA constructs used. An opposite-stranded attachment geometry was prepared, whereby a λ-DNA molecule was tethered to the optically-trapped beads via the 3'-ends on opposite strands. The same-stranded attachment was prepared by tethering the DNA molecule to the beads via the 5' and 3' ends of only one strand. (B) LD as a function of applied force for both opposite- and same-stranded attachment geometries (red circles, and blue x's respectively). (C) Verification procedure for ensuring same-stranded attachment: After fluorescence imaging, the DNA molecule was moved to a low-salt buffer and overstretched to $L/L_C > 1.7$, resulting in peeling of the non-tethered DNA strand from the tethered strand. The red force-extension trace shows the expected saw-tooth pattern during overstretching associated with the peeling process, while the blue trace shows the corresponding curve for single-stranded DNA obtained after retracting the end-to-end length.

3.ii Torsional Constraint Inhibits Intercalator Tilting

We next applied our combined fluorescence polarization and force spectroscopy approach to probe how the tilt angle in overstretched DNA is affected by the presence of torsional constraint. In these experiments, a TC-DNA molecule was generated by tethering an end-capped (i.e. topologically closed) λ-DNA molecule between two optically-trapped beads, via at least two biotin moieties on each end, as described previously [11]. The presence of torsional constraint was verified based on the measured force-extension curve. In contrast to UC-DNA, where the OST is characterized by a plateau at ~65 pN, the OST in TC-DNA occurs at much higher forces, ranging from ~110-130 pN (Fig. 1.D).

We first performed LD measurements on TC-DNA at extensions within the OST ($L/L_c = 1.2 - 1.55$), yielding LD measurements between -0.76 and -0.81, consistent with intercalated dyes oriented nearly perpendicular to the DNA-axis. We then investigated whether intercalator tilting could be detected in TC-DNA at extensions beyond the OST. To this end, we stretched TC-DNA to extensions ranging from $L/L_c = 1.7$ to 1.84 (corresponding to forces between 130 pN and 215 pN). In contrast to UC-DNA, the LD values for TC-DNA beyond the OST exhibited a large magnitude and remained negative, even at extensions well beyond $L/L_c = 1.7$. This indicates that the intercalated dye molecules retained orientations along (or close to) the plane perpendicular to the DNA-axis even as the molecule was extended beyond the end of the OST. Nonetheless, when the DNA was stretched further, to extensions greater than $L/L_c \sim 1.75$ and forces >130 pN (see Fig. 3.A), the LD did eventually begin to decrease in magnitude (*i.e.* become less negative). However, these LD values were still significantly lower than those obtained from UC-DNA at a similar relative extension beyond the OST. For TC-DNA, the highest LD values were between -0.7 and -0.3 (depending upon sequence – see below), with a typical precision of +/- 0.03 LD

units (Fig. 3.A). This contrasts with the UC-DNA results (Fig. 2.B), where the maximum LD reached values between -0.1 and 0.05, with similar measurement precision.

Close inspection of the fluorescence data revealed that the LD values for TC-DNA exhibited reproducible patterns along the length of the DNA construct, in which one half of the DNA molecule displayed a noticeably higher LD than the other half. This pattern correlated well with the known AT/GC-content of λ-DNA, which varies strongly between the two halves of the molecule (see top panel, Fig. 3.D). In contrast, the LD in the case of UC-DNA varied over a much narrower range and showed no significant sequence dependence. To quantify the observed sequence dependence of the LD data in the case of TC-DNA, the transition point between low/high LD regions in each fluorescence image was determined by eye, and the mean LD on either side of the transition point was calculated. These data are shown as a function of force in Fig. 3.A and reveal that AT-rich TC-DNA retains a large magnitude, negative LD of ~ -0.6 even at forces far beyond those encountered within the OST (up to 215 pN), while a more gradual decrease in the LD magnitude occurs as a function of force in the GC-rich portion of the molecule, up to values of ~ -0.35.

In order to confirm that the above results were indeed a consequence of torsional constraint, the following control experiment was performed. Here, a single intercalated TC-DNA molecule was stretched to a relative extension of $L/L_c = 1.78$ (corresponding to a tension of 172 pN). This molecule was repeatedly imaged until a photo-induced nick was generated, and the construct promptly became torsionally unconstrained, resulting in a rapid force-drop of ~20 pN (Fig. 3.B). LD images collected immediately before and after the photo-nick are shown in Fig. 3.C. Before nicking occurred, highly negative LD values were observed, and the magnitude of the LD was strongly correlated with the relative AT/GC-content. However, from the fluorescence images taken

immediately after nicking occurred, the *LD* increased in magnitude to roughly zero (very similar to the values obtained from UC-DNA previously, Fig. 2.B) and no longer exhibited a strong correlation with AT-/GC-rich sequences. An additional example of sequence-dependent *LD* is shown in Fig. S2 in the Supplementary Materials. Note that in this additional example the orientation of the construct is flipped (*i.e*. the GC-rich portion is on the left-side of the molecule).

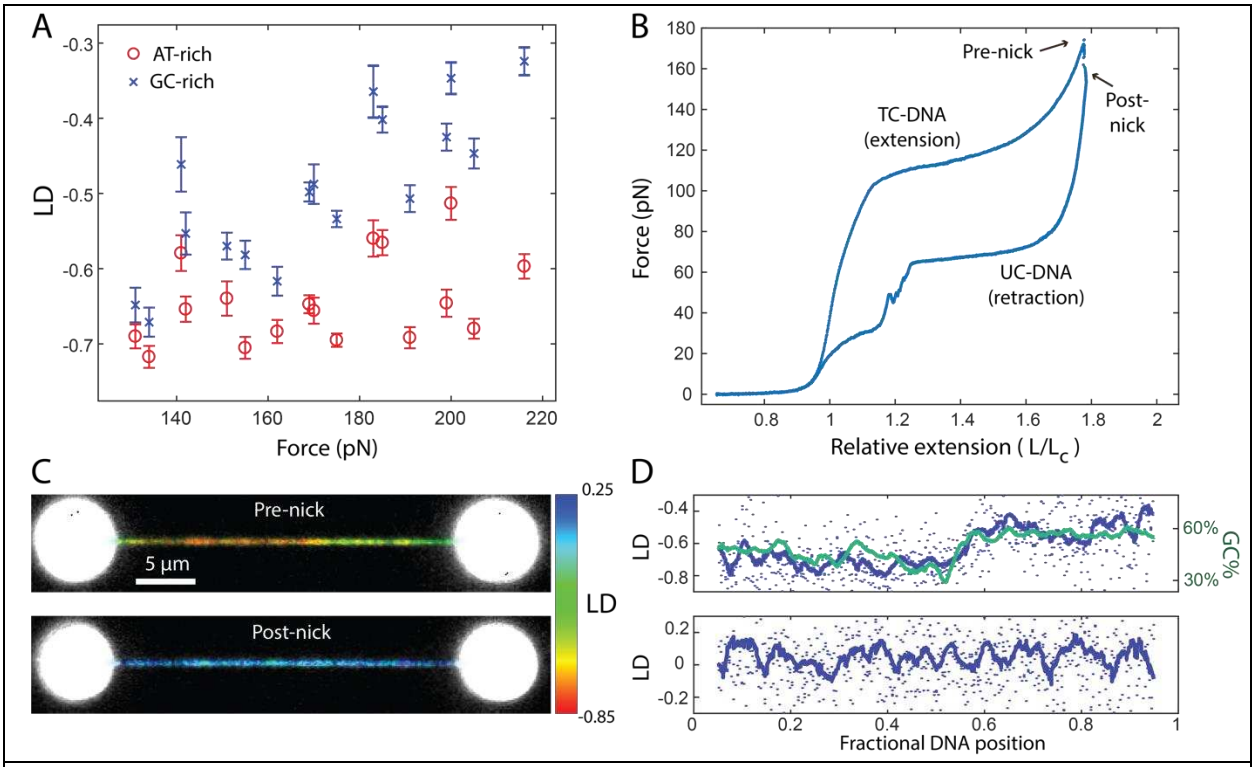

Fig. 3: *LD* measurements for TC-DNA. (A) *LD* for TC-DNA as a function of applied force associated with the AT-rich (red) and GC-rich (blue) regions of the λ-DNA construct. (B) Conversion of TC-DNA to UC-DNA via photo-nicking. The force-extension curve for intercalated TC-DNA is shown prior to the occurrence of a nick. After waiting at ~*L/Lc*~1.75 for a short period of time, a photo-induced nick occurs, resulting in a decrease in the force. The subsequent retraction curve is characteristic of UC-DNA containing a nick. Note that the force–extension behavior associated with intercalated DNA is slightly altered relative to that of bare DNA [12, 13]. (C) Fluorescence polarization images acquired immediately before and after photo-nicking at ~*L/Lc*~1.75. (D) *LD* associated with the fluorescence images before (top) and after (bottom) photo-nicking occurred at ~*L/Lc*~1.75. Smoothed pixelwise data drawn as blue lines. To better illustrate the sequence dependence in the upper image, the re-scaled locally-smoothed percentage of GC base pairs as a function of the position in the DNA molecule is plotted in green.

3.iii Influence of Negative Supercoiling on Intercalator Tilting

We next investigated if, and to what degree, torsional stress influences the orientation of intercalators in TC-DNA. To this end, we generated underwound (negatively supercoiled) DNA, up to a maximum of σ = -0.7, using the recently developed technique of Optical DNA Supercoiling (ODS) [31]. As the supercoiling density increases towards σ = -0.7, an increasingly small fraction of P-DNA is required to off-set the formation of S-DNA during overstretching [9]; beyond σ = -0.7, no P-DNA forms [9, 31]. This raises an intriguing question: how does the presence or absence of P-DNA in negatively supercoiled DNA alter the observed LD? To answer this, we measured the LD over a range of supercoiling densities from σ = 0 to -0.7 at extensions beyond the OST (corresponding to forces of ~150 pN). Surprisingly, no significant difference in intercalator tilting was observed up until at least σ = -0.6, even though only a small fraction of P-DNA remains at this high level of supercoiling (~3% of the entire construct).

The force-extension curves for DNA with σ = -0.6 and -0.7 are shown in the left and middle plots of Fig. 4.A. The corresponding fluorescence polarization data are displayed in the upper two images of Fig. 4.B. At σ = -0.6, we obtained LD values between approximately -0.6 and -0.4 throughout the DNA molecule, largely consistent with the measurements obtained from non-supercoiled TC-DNA under identical conditions (Fig. 3.D). Similar to the case of non-supercoiled TC-DNA, a notable sequence dependence of the LD values was observed for the LD associated with σ = -0.6. The most negative values of LD were obtained in the most AT-rich regions of the molecule (as shown in Fig. 4.C, upper panel, by the left white arrow at the fractional DNA position of approximately 0.55). The LD increases (becomes less negative) in GC-rich regions of the same construct (as indicated in Fig. 4.C, upper panel, by the right white arrow at the fractional DNA position of approximately 0.65). Our LD measurements at a supercoiling density of σ = -0.6 thus

yield similar results to those obtained for non-supercoiled TC-DNA and indicate that even a small fraction of P-DNA causes the intercalated dyes to assume orientations nearly perpendicular to the DNA axis, even at forces beyond the OST. An additional example, showing a DNA molecule with a supercoiling density of σ = -0.25, is shown in Fig. S3. This DNA molecule also exhibits LD values similar to those obtained for TC-DNA.

When the supercoiling density was increased to σ = -0.7 (where no P-DNA was expected), a sudden and drastic change in the measured LD beyond the OST was observed. Here, the LD values were close to 0 throughout the molecule and the LD showed little or no sequence dependence, similar to the results observed for UC-DNA. This similarity was highlighted when the molecule with σ = -0.7 became (accidentally) nicked (due to photo-damage). The occurrence of a nick was determined based on the change in force (yielding a force-extension curve consistent with that of UC-DNA, as shown in the right panel of Fig. 4.A). Upon switching from supercoiled TC-DNA (with σ = -0.7) to UC-DNA, no significant change in LD beyond the OST was observed (see the lower two images in Fig. 4.B and Fig. 4.C). This suggests that in these cases, highly inclined DNA base pairs exist uniformly throughout the entire construct, in contrast to both non-supercoiled TC-DNA and supercoiled TC-DNA with supercoiling densities up to at least σ = -0.6. An additional example of a DNA molecule with a supercoiling density of σ = -0.7 is shown in Fig. S4. This DNA molecule also exhibits LD values indicative of pronounced dipole-tilting.

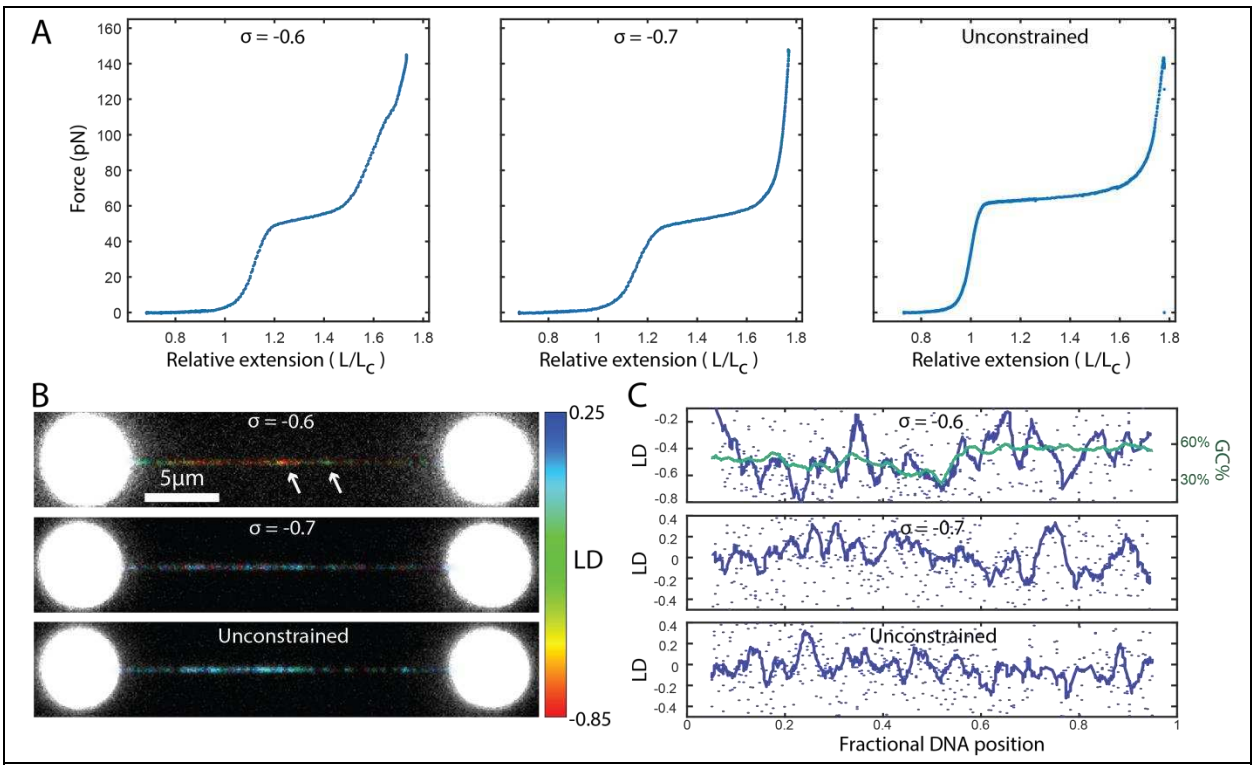

Fig. 4: Comparison of *LD* beyond the OST as a function of negative supercoiling. (A) Sample force-extension curve for a molecule with (left) σ = -0.6, (middle) σ = -0.7 and (right) after photo-nicking of a TC-DNA molecule when it was at σ = -0.7. Note that these curves were recorded sequentially for the same DNA molecule. (B) Fluorescence images showing the *LD* of a DNA molecule at (top) σ = -0.6, (middle) σ =-0.7, and (bottom) after photo-nicking, obtained sequentially from the same molecule. White arrows (top panel) indicate regions of sequence-dependent *LD*. (C) *LD* values obtained from the DNA molecule for each case in panel B as a function of the fractional DNA position.

4. Discussion & Conclusions

In this study, we have used fluorescence polarization microscopy of DNA intercalators to characterize structural features of overstretched DNA arising from pulling geometry, torsional constraint, and negative supercoiling. We first reveal that for intercalated UC-DNA, the LD values at extensions beyond the OST (*i.e.* at forces >100 pN) are close to zero, independent of whether the molecule is overstretched via the same or opposite strands. This result demonstrates that the pronounced ($\theta \sim 54°$) intercalator tilting previously identified beyond the OST for UC-DNA does not depend on the specific pulling geometry but is most likely a direct consequence of the presence of S-DNA. This may, at first, seem surprising, given that several publications have predicted that the pulling geometry can alter DNA structure under tension [29, 30]. Nevertheless, many of these predictions were based on molecular simulations that only considered very short dsDNA constructs (<50bp). Thus, our results could indicate that on much longer constructs (>>10,000 bp), at least, any influence of the pulling geometry is no longer significant. We note that we cannot exclude the possibility that the pulling geometry might have an influence on DNA structural transitions during the OST; however, any effects would have to be sufficiently subtle that we cannot detect them with our approach.

Moreover, we have demonstrated here that intercalated TC-DNA exhibits significantly lower (greater magnitude) LD values beyond the OST than for UC-DNA. This indicates that the intercalated dyes remain oriented near the plane perpendicular to the DNA-axis, even beyond the OST. We also established that, at high forces (>130 pN), the LD values for TC-DNA are sequence dependent: Although the dyes are largely perpendicular to the DNA-axis, they are more tilted in GC-rich regions than in AT-rich regions. Furthermore, we explored the influence of negative supercoiling on intercalator tilting, revealing an intriguing observation: Under conditions where

no P-DNA is present during overstretching ($\sigma = -0.7$), we observe essentially the same *LD* behavior as obtained for UC-DNA, namely intercalator tilting at the end of the OST, with no detectable sequence dependence. Strikingly, however, only a slight decrease in the supercoiling density (from $\sigma = -0.7$ to $\sigma = -0.6$) was sufficient to restore the *LD* features observed for TC-DNA, *i.e*. a greatly reduced intercalator tilting that is sequence dependent.

To explain the observed *LD* measurements on TC-DNA, we first recapitulate one of the conclusions from our earlier work [24]. There, it was noted that a significant depolarization of intercalator fluorescence was observed for UC-DNA only at the very end of the OST. That observation was explained by the assumption that a) the observed depolarization (ascribed to intercalator tilting) is caused by the strongly inclined base pairs associated with the S-DNA conformation and b) there is an energy penalty associated with S-DNA flanking intercalated B-DNA, as has been demonstrated previously [14]. Hence, intercalated DNA is forced to neighbor S-DNA only when B-DNA has disappeared, *i.e*. at extensions beyond the end of the OST, causing the intercalated dyes to assume tilted orientations.

In the case of TC-DNA, there are three relevant DNA conformations to be considered during the OST: B-DNA, S-DNA and P-DNA. While the existence of (overwound) P-DNA is necessary to allow for the formation of (underwound) S-DNA, P-DNA is only present in a small fraction of the molecule. In the absence of supercoiling, the ratio of S-DNA:P-DNA is roughly 4:1. [9, 11]. Since P-DNA is thought to exhibit a base-pair melted structure, in which the bases are flipped outwards [10], we assume that P-DNA will not influence the dye tilt angle at adjacent intercalation sites, and that any neighboring intercalated dyes will have orientations perpendicular to the DNA substrate. This hypothesis is supported by the observation that, beyond the OST, intercalators adopt a less tilted orientation in AT-rich (compared with GC-rich) regions of TC-

DNA. This is consistent with previous suggestions that P-DNA is preferentially formed in AT-rich sequences [11].

While the above assumption that P-DNA will not cause neighboring intercalated dyes to tilt would qualitatively explain a relative decrease in LD (increase in magnitude), this assumption *alone* does not completely account for our observed results. If intercalated dyes were randomly distributed throughout an overstretched TC-DNA construct containing 20% P-DNA (perpendicular dyes) and 80% S-DNA (tilted dyes), this would lead to an estimated LD of approximately -0.12. This calculation is based on our previously developed mathematical model, and experimentally measured tilt-angles and "wobble" cones associated with intercalated UC-DNA extended within and beyond the OST (see the Supplementary Materials of Ref. [24], as well as Refs. [41-46]). If we additionally assume that S-DNA must neighbor both sides of an intercalation site in order to cause significant dipole tilting, this would lead to a construct containing roughly 32% perpendicular dyes and 64% tilted dyes – yielding an estimated LD of only -0.21. In contrast, our measured LD values are significantly lower than this: At the highest forces and extensions for which data were obtained, we recorded an LD of approximately -0.35 and -0.6 for GC-rich DNA, and AT-rich DNA, respectively.

We therefore propose that the most plausible explanation for the greatly reduced tilting measured in TC-DNA beyond the OST is that intercalated dyes are predominantly flanked by P-DNA rather than S-DNA. This hypothesis is further reinforced by the observed dependence of the LD on the supercoiling density. As the density of negative supercoiling is increased, the proportion of P-DNA in the molecules becomes increasingly small. However, even at $\sigma = -0.6$, where only a total fraction (~3%) of P-DNA is assumed to be present [31], we still observed a largely inhibited dye tilting beyond the OST. Only at supercoiling densities of $\sigma = -0.7$, *i.e.*, at conditions where

P-DNA is expected to have completely disappeared, does the measured LD approach the values obtained for UC-DNA. We propose that these observations can be explained by the assumption of a non-stochastic distribution of DNA states in that intercalated DNA is strongly biased towards neighboring P-DNA rather than S-DNA. This is consistent with the large energy penalty that was found previously for intercalated DNA neighboring S-DNA [14], whereas we expect no such penalty for P-DNA. This proposed model is summarized in Fig. 5.A and 5.B.

We note that in all our experiments conducted using TC-DNA, we utilized higher dye concentrations and lower laser illumination powers than in our previous experiments utilizing single YOYO-1 dye molecules (~25-50 nM as opposed to ~1 nM in Ref. [24]). This was a concession made to reduce the probability of photo-nicking over imaging periods lasting on the order of ~2-8 seconds. However, under these conditions we were unable to spatially resolve single intercalated dye molecules. As a result, our reported LD measurements were local ensemble averages over many dyes, and we were unable to detect whether individual intercalators assumed a discrete set of distinct (tilted/un-tilted) orientations, as was found to be the case in Ref. [24]. Despite the increased dye concentration, the dye coverage is below saturation and, at the forces of interest, low enough that we do not expect significant influence on the overstretching characteristics of DNA. In this work, a YOYO-1 concentration of ~25-50 nM was used. In comparison, the experiments in Ref. [24] used YOYO-1 concentrations of ~1 nM in order to give a coverage sufficient to observe discrete single dye molecules (dye distance >> 1 um, corresponding to a coverage of <1 dye molecule for every ~3000 base pairs). Thus, despite the increased YOYO-1 concentration used in the current work, our dye coverage is still very low (expected << 1 dye molecule every 10 base pairs). Furthermore, we note that when the dye coverage is increased, significant distortions in the force-extension curves are observed (see Fig. S5 in the Supplementary Materials). Under the conditions used in our current work, we do observe distortions to the force-extension curve, but these occur at significantly greater relative

extensions within the OST. Due to photo-nicking, we were unable to obtain (emission) polarization-resolved images of TC-DNA stretched along different directions within the image plane. This limitation prevented us from quantitatively estimating probe tilt (θ) without also making assumptions about the extent of probe "wobble" (α). See Ref. [24] for a precise definition of these parameters. Nevertheless, the large magnitude, negative LD values that we obtained for TC-DNA constructs are unambiguous, in that they clearly demonstrate that intercalated dyes must align closer to the plane perpendicular to the DNA-axis than in the case of UC-DNA stretched to similar forces above the OST.

To further substantiate our conclusions, we performed molecular dynamics simulations of bare (unintercalated) UC-DNA and TC-DNA stretched beyond the OST. These constructs were 200 base pairs in length containing AT-rich and GC-rich subregions and being solvated by a continuum model (see the Supplementary Materials). Here, we sought to determine whether structural motifs featuring inclined base pairs would form, in either UC-DNA or TC-DNA upon stretching beyond the OST. In both of these simulated constructs, base-pairing was present in GC-rich regions and exhibited inclinations of $\theta \sim 40° - 50°$ (in comparison, our previous work [24] determined that intercalated dyes in UC-DNA are tilted at $\theta \sim 54°$). However, we caution that our simulations did not recover exact canonical forms of S-DNA and P-DNA. Specifically, base-paired regions in the simulated DNA constructs were overwound relative to the measured helicity of S-DNA (~37.5 bp/turn), and non-base-paired regions were accordingly underwound relative to P-DNA (~2.5 bp/turn). Additionally, more base-pair melting occurred (predominantly in AT-rich DNA) upon overstretching in both the simulated TC-DNA and UC-DNA than would be experimentally expected for our high ionic strength buffer (1M NaCl) [7]. It is not unexpected that we failed to observe purely canonical S- and P-DNA structures from simulations, since the

stretching forces are higher in the simulations and the construct is shorter than in experiments. These constraints are an inevitable consequence of enabling computational tractability for atomic level dynamic precision. Nevertheless, these simulations support our claim that S-DNA contains inclined base pairs, and exists in both TC-DNA and UC-DNA. Building on these promising preliminary findings, we plan to develop further simulations in the future to include the effect of solvent, loading rate and intercalation.

In conclusion, we have shown that combined fluorescence polarization microscopy and DNA force spectroscopy provides a powerful means of investigating nanoscale structural features of overstretched DNA. Our results provide a tantalizing glimpse of the different conformations that form in torsionally constrained DNA under mechanical strain and support previous predictions that these structures are highly sequence-dependent [11, 14, 47]. It is our hope that the new data presented here motivates further inquiry and discussion. More broadly, our current work, alongside emerging techniques in polarization microscopy [48, 49], single-molecule orientation microscopy [50-54], and spatio-angular image-analysis [55, 56] provide a methodological blueprint to non-destructively investigate a wide variety of biological and materials systems.

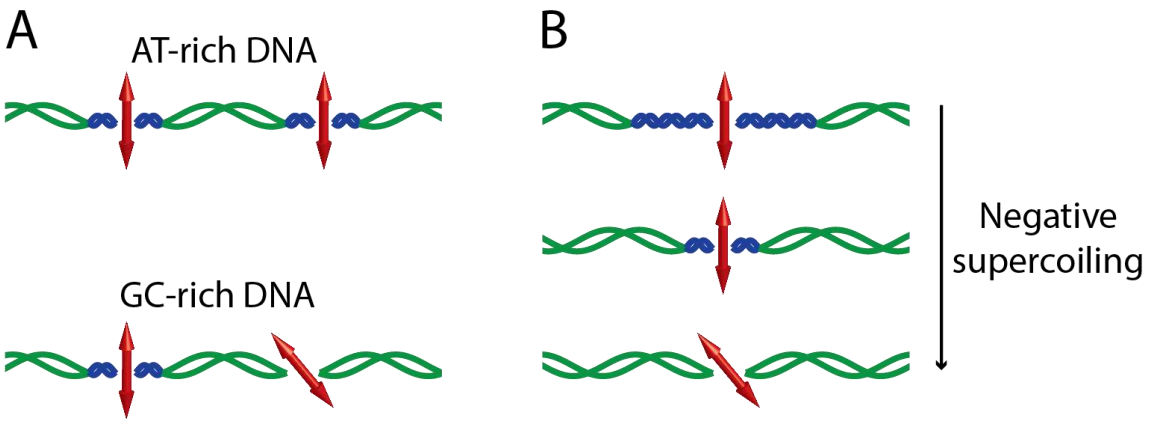

Fig. 5: Proposed mechanisms by which P-DNA inhibits tilting of intercalated dyes during overstretching. P-DNA is depicted in blue, S-DNA in green. Transition dipole moments associated with intercalated dyes are represented as red arrows. For simplicity, DNA bases are not drawn. (A) Due to increased stability of GC relative to AT base-pairing, P-DNA predominantly forms in AT-rich DNA. In AT-rich sections, there is sufficient P-DNA density such that intercalators are allowed to retain the energetically-favored perpendicular orientation. Nevertheless, in GC-rich regions, S-DNA is intermittently "forced" to flank intercalated DNA, leading to sequence-dependent *LD* measurements, and intercalated dipole tilting. (B) Negative supercoiling will reduce the total amount of P-DNA present in overstretched TC-DNA. However, due to the energetic penalty associated with S-DNA flanking intercalated DNA, any remaining P-DNA will preferentially flank intercalation sites. Once a construct approaches a sufficiently negative supercoiling density that P-DNA no longer forms during overstretching, the intercalated dipoles will be tilted (due to being flanked only by S-DNA), and the *LD* will approach values recorded for UC-DNA.

5. Description of Supplementary Materials

The following Supplementary Materials were provided with this manuscript:

- Supplementary Text
- Supplementary Figure S1: Simulations of torsionally constrained and unconstrained DNA
- Supplementary Figure S2: Additional example of sequence-dependent LD in a TC-DNA molecule
- Supplementary Figure S3: Additional example of a partially supercoiled DNA molecule
- Supplementary Figure S4: Additional example of a fully supercoiled DNA molecule
- Supplementary Figure S5: Effect of dye coverage on TC-DNA force versus extension behavior
- Supplementary References

6. Acknowledgements

Funding: Data appearing in this manuscript were collected while A.S.Ba. was an employee of Sandia National Laboratories. A.S.Ba. acknowledges support from the Laboratory Directed Research and Development program, and the Harry S. Truman Fellowship at Sandia. This work was supported by a Chemical Sciences Top grant from the Netherlands Organization for Scientific Research (NWO) (G.J.L.W. and E.J.G.P. and G.A.K.). I.H. acknowledges research funding from an NWO VIDI award. M.C.L. acknowledges the Leverhulme Trust, U.K. (RPG-2017-340, RPG-2019-156), and the Engineering and Physical Sciences Research Council, U.K. (EPSRC, EP/N027639/1) (A.N. and M.C.L.), with computational time secured on JADE via the U.K. High-End Computing Consortium for Biomolecular Simulation, HECBioSim (EP/R029407/1) (A.N.) and on the Cambridge Tier-2 system capital grant (EP/P020259/1) (A.N.). We also thank Tier 3 High Performance Computing (HPC) facilities at the University of York, U.K. (Viking cluster) for additional computational resources. **Competing interests:** A.S.Ba., G.A.K., A.S.Bi., J.W.S., A.N., and M.C.L. declare no competing financial interest. The combined optical tweezers fluorescence microscopy technology is licensed to LUMICKS b.v., in which I.H., G.J.L.W. and E.J.G.P. have a financial interest.

7. References

1. Cluzel, P.; Lebrun, A.; Heller, C.; Lavery, R.; Viovy, J. L.; Chatenay, D.; Caron, F. DNA: An extensible molecule. *Science* **1996**, *271*, 792-794.
2. Smith, S. B.; Cui, Y.; Bustamante, C. Overstretching B-DNA: The elastic response of individual double-stranded and single-stranded DNA molecules. *Science* **1996**, *271*, 795-799.
3. Cocco, S.; Yan, J.; Léger, J. F.; Chatenay, D.; Marko, J. F. Overstretching and force-driven strand separation of double-helix DNA. *Phys. Rev. E* **2004**, *70*, 011910.
4. van Mameren, J.; Gross, P.; Farge, G.; Hooijman, P.; Modesti, M.; Falkenberg, M.; Wuite, G. J. L.; Peterman, E. J. G. Unraveling the structure of DNA during overstretching by using multicolor, single-molecule fluorescence imaging. *Proc. Natl. Acad. Sci. USA* **2009**, *106*, 18231-18236.
5. Gross, P.; Laurens, N.; Oddershede, L. B.; Bockelmann, U.; Peterman, E. J. G.; Wuite, G. J. L. Quantifying how DNA stretches, melts, and changes twist under tension. *Nat. Phys.* **2011**, *7*, 731-736.
6. Bosaeus, N.; El-Sagheer, A.; Brown, T.; Smith, S. B.; Åkerman, B.; Bustamante, C.; Nordén, B. Tension induces a base-paired overstretched DNA conformation. *Proc. Natl. Acad. Sci. USA* **2012**, *109*, 15179-15184.

7. King, G. A.; Gross, P.; Bockelmann, U.; Modesti, M.; Wuite, G. J. L.; Peterman, E. J. G. Revealing the competition between peeled ssDNA, melting bubbles, and S-DNA during DNA overstretching using fluorescence microscopy. *Proc. Natl. Acad. Sci. USA* **2013**, *110*, 3859-3864.
8. Zhang, X.; Chen, H.; Le, S.; Rouzina, I.; Doyle, P. S.; Yan, J. Revealing the competition between peeled ssDNA, melting bubbles, and S-DNA during DNA overstretching by single-molecule calorimetry. *Proc. Natl. Acad. Sci. USA* **2013**, *110*, 3865-3870.
9. Léger, J. F.; Romano, G.; Sarkar, A.; Robert, J.; Bourdieu, L.; Chatenay, D.; Marko, J. F. Structural transitions of a twisted and stretched DNA molecule. *Phys. Rev. Lett.* **1999**, *83*, 1066-1069.
10. Allemand, J. F.; Bensimon, D.; Lavery, R.; Croquette, V. Stretched and overwound DNA forms a Pauling-like structure with exposed bases. *Proc. Natl. Acad. Sci. USA* **1998**, *95*, 14152-14157.
11. King, G. A.; Peterman, E. J. G.; Wuite, G. J. L. Unraveling the structural plasticity of stretched DNA under torsional constraint. *Nat. Commun.* **2016**, *7*, 11810.
12. Vladescu, I. D.; McCauley, M. J.; Nuñez, M. E.; Rouzina, I.; Williams, M. C. Quantifying force-dependent and zero-force DNA intercalation by single-molecule stretching. *Nat. Methods* **2007**, *4*, 517-522.
13. Biebricher, A. S.; Heller, I.; Roijmans, R. F. H.; Hoekstra, T. P.; Peterman, E. J. G.; Wuite, G. J. L. The impact of DNA intercalators on DNA and DNA-processing enzymes elucidated through force-dependent binding kinetics. *Nat. Commun.* **2015**, *6*, 7304.
14. Schakenraad, K.; Biebricher, A. S.; Sebregts, M.; ten Bensel, B.; Peterman, E. J. G.; Wuite, G. J. L.; Heller, I.; Storm, C.; van der Schoot, P. Hyperstretching DNA. *Nat. Commun.* **2017***, 8*, 2197.
15. Lerman, L. S. Structural considerations in the interaction of DNA and acridines. *J. Mol. Biol.* **1961***, 3*, 18-30.
16. Glazer, A. N.; Rye, H. S. Stable dye-DNA intercalation complexes as reagents for high-sensitivity fluorescence detection. *Nature* **1992***, 359*, 859-861.
17. Carlsson, C.; Larsson, A.; Jonsson, M.; Albinsson, B.; Nordén, B. Optical and photophysical properties of the oxazole yellow DNA probes YO and YOYO. *J. Phys. Chem.* **1994**, *98*, 10313-10321.
18. Larsson, A.; Carlsson, C.; Jonsson, M.; Albinsson, B. Characterization of the binding of the fluorescent dyes YO and YOYO to DNA by polarized light spectroscopy. *J. Am. Chem. Soc.* **1994**, *116*, 8459-8465.
19. Bennink, M. L.; Schärer, O. D.; Kanaar, R.; Sakata-Sogawa, K.; Schins, J. M.; Kanger, J. S.; de Grooth, B. G.; Greve, J. Single-molecule manipulation of double-stranded DNA using optical tweezers: Interaction studies of DNA with RecA and YOYO-1. *Cytom. A* **1999**, *36*, 200-208.
20. Murade, C. U.; Subramanianm, V.; Otto, C.; Bennink, M. L. Force spectroscopy and fluorescence microscopy of dsDNA-YOYO-1 complexes: implications for the structure of dsDNA in the overstretching region. *Nucleic Acids Res.* **2010**, *38*, 3423-3431.
21. Valades-Cruz, C. A.; Shaban, H. A.; Kress, A.; Bertaux, N.; Monneret, S.; Mavrakis, M.; Savatier, J.; Brasselet, S. Quantitative nanoscale imaging of orientational order in biological filaments by polarized superresolution microscopy. *Proc. Natl. Acad. Sci. USA* **2016**, *113*, E820-E828.
22. Backer, A. S.; Lee, M. Y.; Moerner, W. E. Enhanced DNA imaging using super-resolution microscopy and simultaneous single-molecule orientation measurements. *Optica* **2016**, *3*, 659-666.
23. van Mameren, J.; Vermeulen, K.; Wuite, G. J. L.; Peterman, E. J. G. A polarized view on DNA under tension. *J. Chem. Phys.* **2018**, *148*, 123306.
24. Backer, A. S.; Biebricher, A. S.; King, G. A.; Wuite, G. J. L.; Heller, I.; Peterman, E. J. G. Single-molecule polarization microscopy of DNA intercalators sheds light on the structure of S-DNA. *Sci. Adv.* **2019**, *5*, eaav1083.
25. Lebrun, A.; Lavery, R. Modelling extreme stretching of DNA. *Nucleic Acids Res.* **1996**, *24*, 2260-2267.

26. Konrad, M. W.; Bolonick, J. I. Molecular dynamics simulation of DNA stretching is consistent with the tension observed for extension and strand separation and predicts a novel ladder structure. *J. Am. Chem. Soc.* **1996**, *118*, 10989-10994.
27. Kosikov, K. M.; Gorin, A. A.; Zhurkin, V. B.; Olson, W. K. DNA stretching and compression: Large-scale simulations of double helical structures. *J. Mol. Biol.* **1999***, 289*, 1301-1326.
28. Prévost, C.; M. Takahashi, M.; Lavery, R. Deforming DNA: from physics to biology. *ChemPhysChem* **2009**, *10*, 1399-1404.
29. Danilowicz, C.; Limouse, C.; Hatch, K.; Conover, A.; Colijee, V. W.; Kleckner, N.; Prentiss, M. The structure of DNA overstretched from the 5'5' ends differs from the structure of DNA overstretched from the 3'3' ends. *Proc. Natl. Acad. Sci. USA* **2009**, *106*, 13196-13201.
30. Bosaeus, N.; Reymer, A.; Beke-Somfai, T.; Brown, T.; Takahashi, M.; Wittung-Stafshede, P.; Rocha, S.; Nordén, B. A stretched conformation of DNA with a biological role? *Q. Rev. Biophys.* **2017**, *50***,** e11.
31. King, G. A.; Burla, F.; Peterman, E. J. G.; Wuite, G. J. L. Supercoiling DNA Optically. *Proc. Natl. Acad. Sci. USA* **2019**, *116*, 26534-26539.
32. Sarlós, K.; Biebricher, A. S.; Bizard, A. H.; Bakx, J. A. M.; Ferreté-Bonastre, A. G.; Modesti, M.; Paramasivam, M.; Yao, Q.; Peterman, E. J. G.; Wuite, G. J. L.; et al. Reconstitution of anaphase DNA bridge recognition and disjunction. *Nat. Struct. Mol. Biol.* **2018**, *25*, 868-876.
33. Ha, T.; Enderle, Th.; Chemla, D. S.; Selvin, P. R.; Weiss, S. Single molecule dynamics studied by polarization modulation. *Phys. Rev. Lett.* **2019***, 77*, 3979.
34. Sosa, H.; Peterman, E. J. G.; Moerner, W. E.; Goldstein, L. S. B. ADP-induced rocking of the kinesin motor domain revealed by single-molecule fluorescence polarization microscopy. *Nat. Struct. Mol. Biol.* **2001**, *8*, 540-544.
35. Peterman, E. J. G.; Sosa, H.; Goldstein, L. S. B.; Moerner, W. E. Polarized fluorescence microscopy of individual and many kinesin motors bound to axonemal microtubules. *Biophys. J.* **2001***, 81*, 2851-2863.
36. Gross, P.; Farge, G.; Peterman, E. J. G.; Wuite, G. J. L. Combining optical tweezers, single-molecule fluorescence microscopy, and microfluidics for studies of DNA-Protein interactions. *Methods Enzymol.* **2010***, 475*, 427-453.
37. Candelli, A.; Hoekstra, T. P.; Farge, G.; Gross, P.; Peterman, E. J. G.; Wuite, G. J. L. A toolbox for generating single-stranded DNA in optical tweezers experiments. *Biopolymers* **2013**, *99*, 611-620.
38. https://www.mathworks.com/help/signal/ref/sgolayfilt.html (accessed on March 21, 2021).
39. Sanger, F.; Coulson, A. R.; Hong, G. F.; Hill, D. F.; Petersen, G. B. Nucleotide sequence of bacteriophage λ DNA. *J. Mol. Biol.* **1982**, *162*, 729-773.
40. https://www.mathworks.com/help/stats/analysis-of-variance-and-covariance.html (accessed on March 21, 2021).
41. Axelrod, D. Carbocyanine dye orientation in red cell membrane studied by microscopic fluorescence polarization. *Biophys. J.* **1979**, *26*, 557-573.
42. Irving, M. Steady-state polarization from cylindrically symmetric fluorophores undergoing rapid restricted motion. *Biophys. J.* **1996**, *70*, 1830-1835.
43. Dickson, R. M.; Norris, D. J.; Moerner, W. E. Simultaneous imaging of individual molecules aligned both parallel and perpendicular to the optic axis. *Phys. Rev. Lett.* **1998**, *81*, 5322-5325.
44. Böhmer, M.; Enderlein, J. Orientation imaging of single molecules by wide-field epifluorescence microscopy. *J. Opt. Soc. Am. B* **2003**, *20*, 554-559.
45. Backer, A. S.; Moerner, W. E. Extending single-molecule microscopy using optical Fourier processing. *J. Phys. Chem. B* **118**, 8313-8329 (2014).
46. Shroder, D. Y.; Lippert, L. G.; Goldman, Y. E. Single molecule optical measurements of orientation and rotations of biological macromolecules. *Methods Appl. Fluoresc.* **2016***, 4*, 042004.

47. Shepherd, J. W.; Greenall, R. J.; Probert, M. I. J.; Noy, A.; Leake, M. C. The emergence of sequence-dependent structural motifs in stretched, torsionally-constrained DNA. *Nucleic Acids Res.* **2020**, *48*, 1748-1763.
48. Brockman, J. M.; Blanchard, A. T.; Ma, V. P.; Derricotte, W. D.; Zhang, Y.; Fay, M. E.; Lam, W. A.; Evangelista, F. A.; Mattheyses, A. L.; Salaita, K. Mapping the 3D orientation of piconewton integrin traction forces. *Nat. Methods* **2018**, *15*, 115-118.
49. Zhanghao, K.; Chen, X.; Liu, W.; Li, M; Liu, Y.; Wang, Y.; Luo, S.; Wang, X.; Shan, C.; Xie, H.; et al. Super-resolution imaging of fluorescent dipoles via polarized structured illumination microscopy. *Nat. Commun.* **2019**, *10*, 4694.
50. Mehta, S. B.; McQuilkin, M.; La Rivière, P. J.; Occhipinti, P.; Verma, A.; Oldenbourg, R.; Gladfelter, A. S.; Tani, T. Dissection of molecular assembly dynamics by tracking orientation and position of single molecules in live cells. *Proc. Natl. Acad. Sci. USA* **2016**, *113*, E6352-E6361.
51. Ding, T.; Wu, T.; Mazidi, H.; Zhang, O.; Lew, M. D. Single-molecule orientation localization microscopy for resolving structural heterogeneities between amyloid fibrils. *Optica* **2020**, *7*, 602-607.
52. Lu, J.; Mazidi, H.; Ding, T.; Zhang, O.; Lew, M. D. Single-molecule orientation imaging reveals nanoscale compositional heterogeneity in lipid membranes. *Angew. Chem. Int.* **2020**, *59*, 17572-17579.
53. Curcio, V.; Alemán-Castañeda, L. A.; Brown, T. G.; Brasselet, S.; Alonso, M. A. Birefringent Fourier filtering for single molecule coordinate and height super-resolution imaging with dithering and orientation. *Nat. Commun.* **2020***, 11*, 5307.
54. Hulleman, C. N.; Thorsen, R. Ø.; Stallinga, S.; Rieger, B. Simultaneous orientation and 3D localization microscopy with a vortex point spread function. *bioRxiv* **2020,** doi: 10.1101/2020.10.01.322834.
55. Chandler, T.; Shroff, H.; Oldenbourg, R.; La Rivière, P. Spatio-angular fluorescence microscopy I: basic theory. *J. Opt. Soc. Am. A* **2019***, 36*, 1334-1345.
56. Zhang, O.; Lew, M. D. Fundamental limits on measuring the rotational constraint of single molecules using fluorescence microscopy. *Phys. Rev. Lett.* **2019**, *122*, 198301.

TOC Graphic

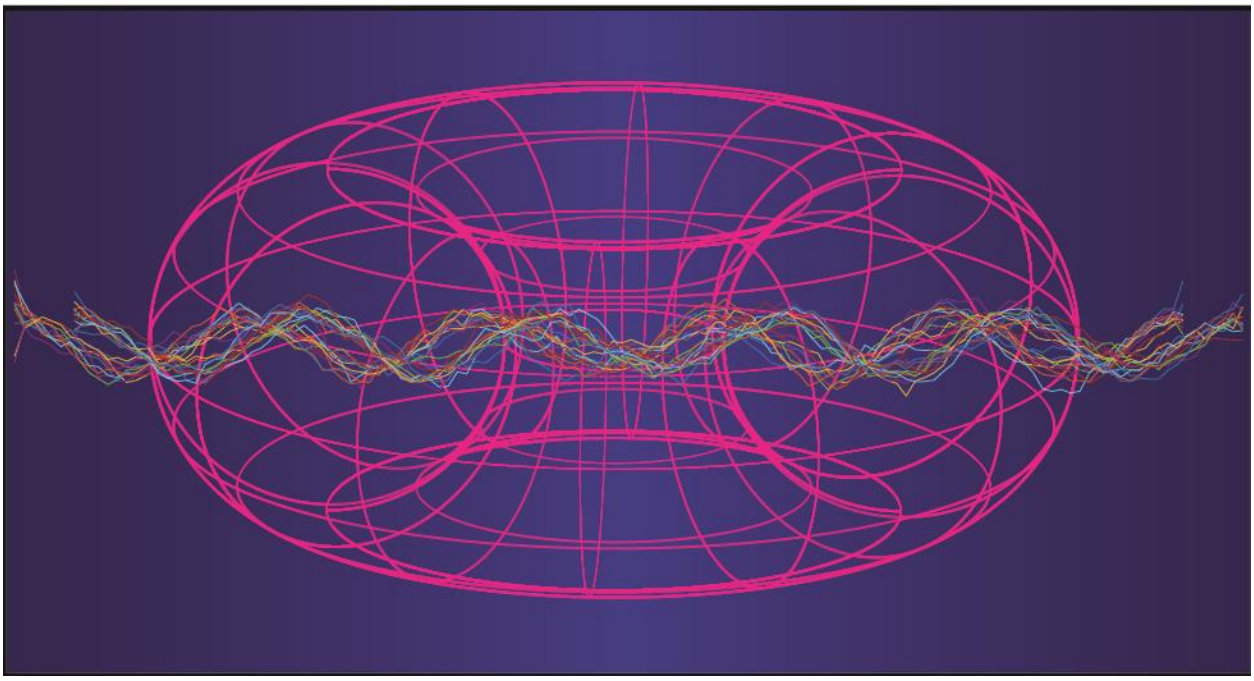

Supplementary Materials

Elucidating the Role of Topological Constraint on the Structure of Overstretched DNA using Fluorescence Polarization Microscopy

Invited submission to the W. E. Moerner Festschrift Special Issue

Adam S. Backer[1,*], Graeme A. King[2], Andreas S. Biebricher[3], Jack W. Shepherd[4,5], Agnes Noy[4], Mark C. Leake[4,5], Iddo Heller[3], Gijs J. L. Wuite[3], and Erwin J. G. Peterman[3,*]

[1]Apple Inc., 1 Apple Park Way, Cupertino, CA 95014, USA
[2]Institute of Structural and Molecular Biology, University College London, Gower Street, London WC1E 6BT, UK
[3]Department of Physics and Astronomy, LaserLaB Amsterdam, Vrije Universiteit Amsterdam, De Boelelaan 1081, 1081 HV Amsterdam, The Netherlands
[4]Department of Physics, University of York, York, YO10 5DD, UK
[5]Department of Biology, University of York, York, YO10 5DD, UK

*Correspondence should be addressed to both Adam S. Backer (email: a.s.backer@gmail.com) and Erwin J. G. Peterman (email: e.j.g.peterman@vu.nl)

Contents

Supplementary Text

Summary

We present simulations on bare, torsionally constrained and unconstrained DNA constructs extended to 1.72x their contour length. In both stretching simulations, we observed the co-existence of two main structural motifs: S-DNA-like structures in GC-rich regions containing inclined base pairs, and P-DNA-like/melted structures in AT-rich sequences with the two backbones collapsed and the bases pointing outside.

Supplementary Methods

Simulations of torsionally constrained and unconstrained DNA were performed similarly to simulations previously reported [1]. A DNA sequence 200 bp in length was constructed using Python to give a random sequence with specified AT and GC content, 100 bp of 60% AT followed by 100 bp of 60% GC. The sequence was passed to Amber's nab utility which created a dual-strand DNA fragment in the canonical fiber-diffraction B-DNA structure. tleap was used to construct topology and co-ordinate files from the resulting PDB file. Simulations were run using Amber18's pmemd.cuda [2].

For torsionally constrained DNA, both terminal base pairs were held in place with harmonic constraints and one terminal base pair was moved 1 Å between each umbrella sampling window, each of which were 1 ns long with an integration time of 1 fs. For torsionally unconstrained DNA, only the 3' nucleotides were held fixed and moved to simulate 3'-3' stretching by optical tweezers. Simulations were performed in implicit Generalized Born solvation [3] with effective salt concentration 1 M (emulating experimental conditions reported in the main text). 450 umbrella sampling windows were performed for each simulation giving an overall maximum extension L/L_C of 1.72.

The full simulations were used to construct heatmaps of Watson-Crick base pairing as performed previously using Amber's cpptraj [4]. For both torsionally constrained and unconstrained DNA the final umbrella sampling window was used to generate an average structure which was analyzed for inclination using Curves+ [5]. Curves+ was used to estimate the inclination of each nucleotide individually. In the case of hydrogen bonded base pairs (i.e. with Watson-Crick occupancy >1 for AT base pairs and >1.5 for CG base pairs) the single nucleotide inclinations were averaged to produce an approximate base-pair inclination. Unpaired bases were neglected here and in the average inclination calculation. Finally, structures were visualized using VMD [6].

Supplementary Results

Both the unconstrained and constrained stretching simulations showed significant loss of hydrogen bonding throughout the calculation, as seen in Figs. S1.B and S1.D. In each case, the percentage of base-paired AT and CG base pairs is approximately the same, at around 80% for CG and 10% for AT. For the torsionally unconstrained simulation, however, more hydrogen bonds remain to the end of the simulation, presumably as the DNA is able to relax torsionally rather than break hydrogen bonds to absorb the increasing overextension. As would be expected, in each case the hydrogen bond loss is higher in the 60% AT region, reflecting the A-T base pair's weaker interaction. It is worth saying that all these results might present a bias towards melted structures compared with what has been previously suggested [7] due to the approximate representation of the solvent.

In both torsionally constrained and unconstrained simulations, after extension to $L/L_C = 1.72$, average inclination of the remaining intact base pairs is around 50 degrees, roughly similar to the dye orientations estimated in [8] (~54°) (see Fig. S1.A and S1.C). This tilting is related to S-DNA-like structures observed in CG rich areas in our simulations, where base pairs are intact

but relatively inclined compared with B-DNA (Fig. S1.E). The other structural motifs observed are P-DNA-like structures, which are prominent in AT-rich sequences and where the phosphate backbone effectively collapses while the nucleotides themselves are exposed to solution (Fig. S1.F). Although the broad aspect of these structural motifs agree with the experimental hypothesis, the description of the fine details reasonably needs a more accurate representation of the solvent and especially of the ions which in the Generalized Born method are modelled as a continuum but which can intercalate and interact with specific sites in some biomolecules. However, the coexistence of these motifs provides more evidence to support the hypothesized overstretching pathway for torsionally constrained DNA (Fig. 5, main text). The simulations presented here are also under an effectively much higher loading rate than experiments, and the umbrella sampling window is necessarily shorter than an experimental timescale, both of which may impact the structures observed. It is also important to point out that these simulations did not attempt to model intercalated YOYO-1 within the overstretched DNA and the study of this particular effect will require future computational investigation. Further simulations of DNA fragments with intercalated YOYO-1 might further elucidate the hypothesis that P-DNA flanks intercalated DNA and serves to inhibit dye-tilting, as reported experimentally in the main text.

Supplementary Figures

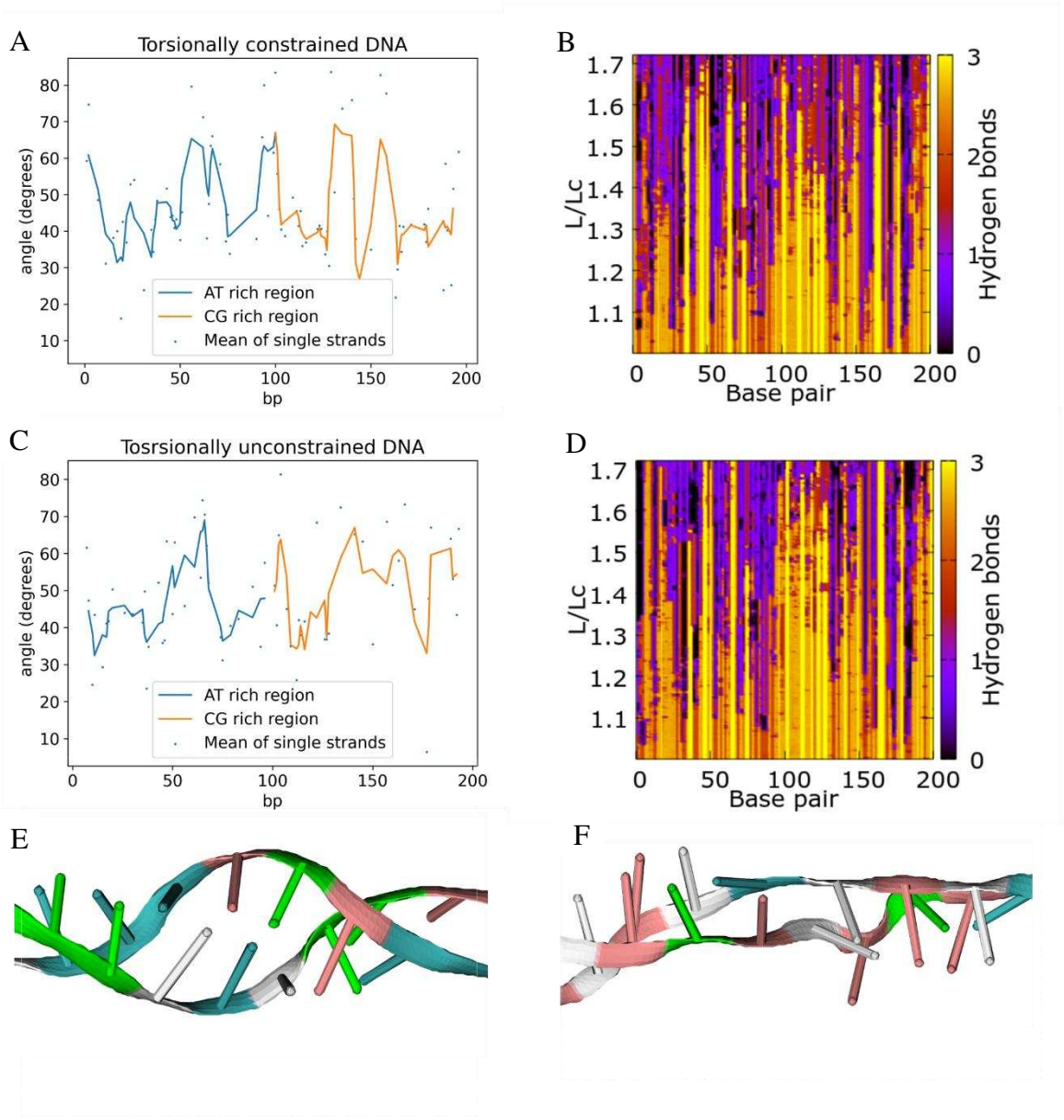

Supplementary Figure S1. Simulations of torsionally constrained and unconstrained DNA. (A) base pair inclination as measured as an average of nucleotide inclination in unmelted base pairs for the torsionally constrained simulation at $L/L_C = 1.7$. A rolling average of 3 data points corresponding to approximately 10 base pairs is shown with solid lines. (B) Watson-Crick hydrogen bonds present throughout the torsionally constrained simulation. (C) base pair inclinations as measured in panel A for the torsionally unconstrained simulation at $L/L_C = 1.7$. (D) heatmap of the number of Watson-Crick hydrogen bonds present throughout the torsionally unconstrained stretching simulation. (E) S-DNA apparent at $L/L_C = 1.7$ in torsionally constrained DNA. (F) P-DNA-like structures in torsionally constrained DNA with $L/L_C = 1.7$. A in white, T in peach, G in blue and C in green.

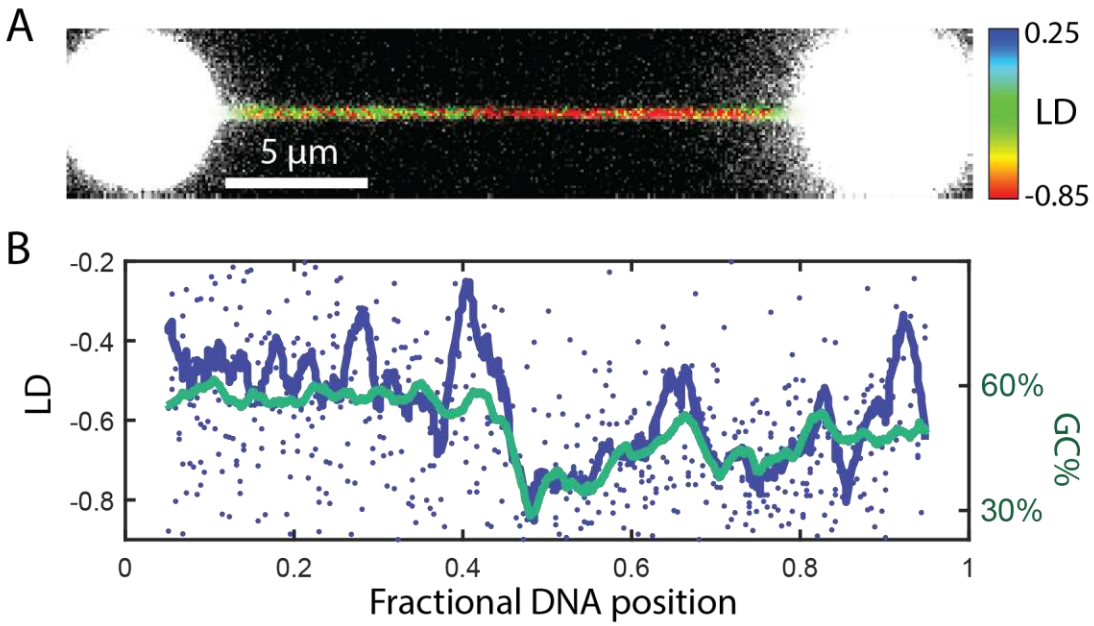

Supplementary Figure S2. Additional example of sequence-dependent LD in a TC-DNA molecule. (A) Fluorescence polarization image of a TC-DNA molecule extended to $L/L_C \sim 1.83$ and 191 pN of force. (B) Pixelwise LD measurements plotted according to their fractional position along the DNA construct. Smoothed data is drawn as a blue line. To illustrate sequence dependence, the re-scaled locally-smoothed percentage of GC base pairs is also plotted, as described in the main text. Note that in this example, the GC-rich portion of the DNA is on the left side of the molecule, while in the example given in the main text, the GC-rich portion is on the right side-- indicating opposite-ended attachment of the DNA to the optically-trapped beads.

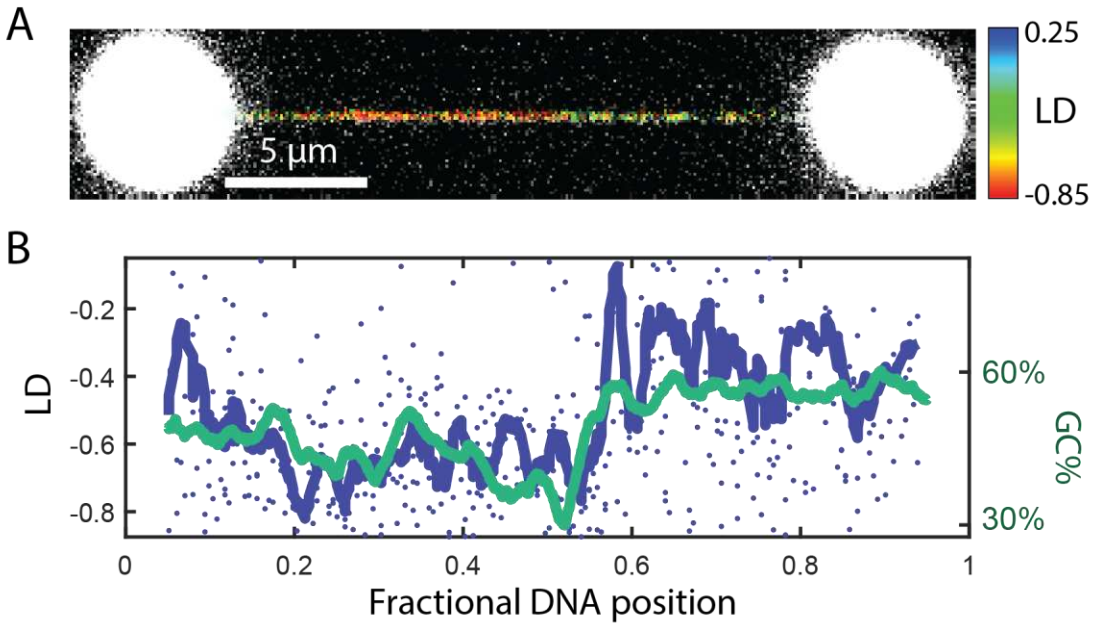

Supplementary Figure S3. Additional example of a partially supercoiled DNA molecule. (A) Fluorescence polarization image shows LD measurements (between roughly -0.8 and -0.2) similar to those obtained for (un-supercoiled) TC-DNA. (B) Pixelwise and smoothed LD measurements plotted according to their fractional position along the DNA construct. The locally-smoothed GC base-pair percentage is plotted on the same axes. In this example, images were recorded at an extension of $L/L_C \sim 1.76$ and 147 pN of force. The supercoiling density was estimated as described in the main text to be $\sigma \sim -0.25$.

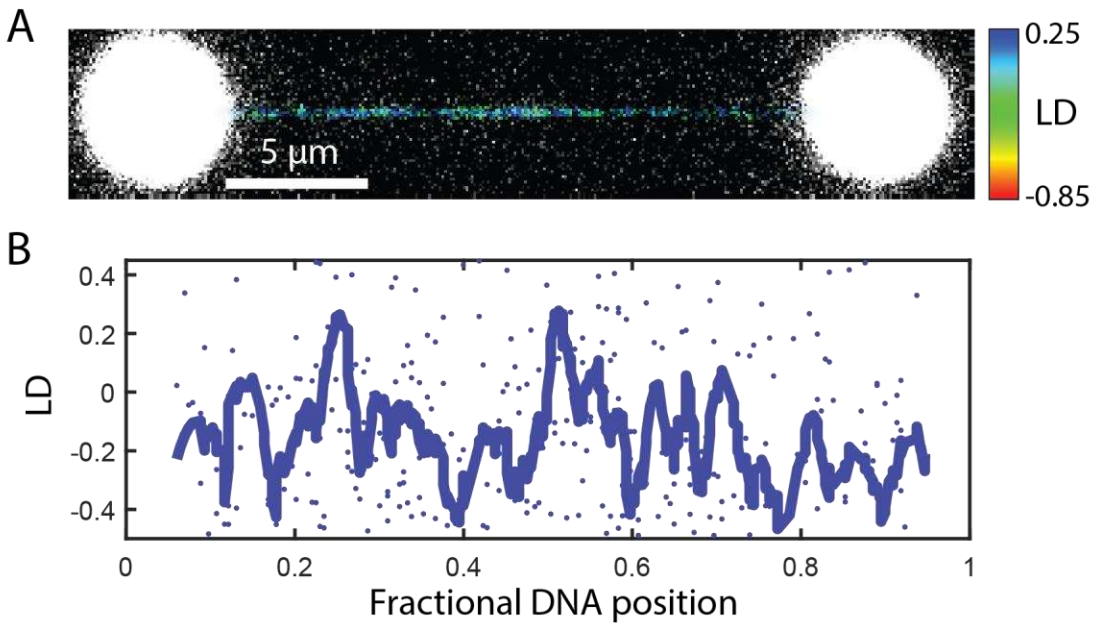

Supplementary Figure S4. Additional example of a fully supercoiled DNA molecule ($\sigma \sim -0.7$). (A) Fluorescence polarization image shows LD measurements (between roughly -0.3 and 0.1) similar to those obtained for torsionally unconstrained DNA, and significantly higher than values recorded at lower supercoiling densities. (B) Pixelwise and smoothed LD measurements plotted according to their fractional position along the DNA construct. In this example, images were recorded at an extension of $L/L_C \sim 1.73$ and 88 pN of force.

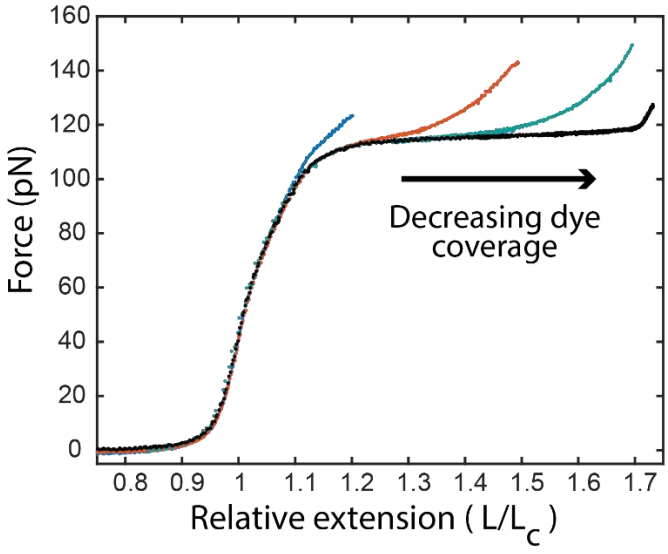

Supplementary Figure S5. Effect of dye coverage on TC-DNA force versus extension behavior. A TC-DNA molecule was repeatedly extended in the presence of different concentrations of YOYO-1 dye. At increasing dye coverage, deviations from the bare DNA overstretching curve (black curve) occur at lower relative extension. Fluorescence polarization measurements were taken for dye coverages that yielded force versus extension curves most closely resembling the green curve shown above. At this concentration, We estimate that YOYO-1 coverage was no more than ~ 1 dye / 10 bp, and was significantly below saturation.

Supplementary References

[1] J. W. Shepherd, R. J. Greenall, M. I. J. Probert, A. Noy, and M. C. Leake, "The emergence of sequence-dependent structural motifs in stretched, torsionally constrained DNA," *Nucleic Acids Res.*, 2020, doi: 10.1093/nar/gkz1227.

[2] L. Vinet and A. Zhedanov, "A 'missing' family of classical orthogonal polynomials," *Journal of Physics A: Mathematical and Theoretical*, vol. 44, no. 8. 2011, doi: 10.1088/1751-8113/44/8/085201.

[3] H. Nguyen, A. Pérez, S. Bermeo, and C. Simmerling, "Refinement of Generalized Born Implicit Solvation Parameters for Nucleic Acids and Their Complexes with Proteins," *J. Chem. Theory Comput.*, vol. 11, no. 8, pp. 3714–3728, 2015, doi: 10.1021/acs.jctc.5b00271.

[4] D. R. Roe and T. E. Cheatham, "PTRAJ and CPPTRAJ: Software for processing and analysis of molecular dynamics trajectory data," *J. Chem. Theory Comput.*, vol. 9, no. 7, pp. 3084–3095, 2013, doi: 10.1021/ct400341p.

[5] R. Lavery, M. Moakher, J. H. Maddocks, D. Petkeviciute, and K. Zakrzewska, "Conformational analysis of nucleic acids revisited: Curves+," *Nucleic Acids Res.*, vol. 37, no. 17, pp. 5917–5929, 2009, doi: 10.1093/nar/gkp608.

[6] W. Humphrey, A. Dalke, and K. Schulten, "VMD: Visual molecular dynamics," *J. Mol. Graph.*, vol. 14, no. 1, pp. 33–38, 1996, doi: 10.1016/0263-7855(96)00018-5.

[7] G. King, P. Gross, U. Bockelmann, M. Modesti, G. Wuite, E. Peterman, "Revealing the competition between peeled ssDNA, melting bubbles, and S-DNA during DNA overstretching using fluorescence microscopy," vol. 110, no. 10, pp. 3859-3864, 2013, doi: 10.1073/pnas.1213676110.

[8] A. Backer, A. Biebricher, G. King, G. Wuite, I. Heller and E. Peterman, "Single-molecule polarization microscopy of DNA intercalators sheds light on the structure of S-DNA," *Sci. Adv.* vol. 5, no. 3, eaaav1083, 2019, doi: 10.1126/sciadv.aav1083.